2017

# Development of a Low-Energy Monoenergetic Electron Separator

Sergio Martín López Cáceres
*Louisiana State University and Agricultural and Mechanical College*

# DEVELOPMENT OF A LOW-ENERGY MONOENERGETIC ELECTRON SEPARATOR

A Thesis

Submitted to the Graduate Faculty of the
Louisiana State University and
Agricultural and Mechanical College
in partial fulfillment of the
requirements for the degree of
Master of Science

in

The Department of Physics and Astronomy

by
Sergio Martín López Cáceres
B.S., Universidad Nacional de Asunción, 2007
August 2017

ACKNOWLEDGEMENTS

This project could not have been possible without the help of some people. Among them, I would very much like to thank my thesis advisor, Dr. Scott Marley. His constant help throughout the project, his insightful comments and remarks, his patience during the writing and experiments, and his engaged spirit, made possible the realization of this thesis on a timely fashion.

I would also like to thank the people in the LSU Physics and Astronomy Machine shop, who even though were loaded with work, made an effort to finish components on time. I cannot forget to thank as well the people in the Physics and Astronomy Electronics shop who were always available to suggest ways to have the best cable connections.

Finally, I thank the Nuclear Physics group for the harmonious working environment that made possible this project to be carried without interruptions.

TABLE OF CONTENTS

LIST OF FIGURES

## ABSTRACT

The aim of this project is to build a prototype device that can select electrons of certain energy in order to have a monoenergetic beam suitable for the characterization of radiation detectors. Current options for sources of electrons are either from radioisotopes or accelerator facilities. Radioisotope sources are not tunable in energy since they depend on the nuclear and atomic structures of the daughter nucleus. On the other hand, even though accelerators offer the feature of a variable energy beam, they have limited availability and are not typically run at low intensities. Therefore, the motivation for this thesis is the development of a “table top” device that can be used in the laboratory.

Theoretical calculations were performed for the design of the vacuum chamber and the magnet array. Magnetic field mapping was performed between magnets to check for uniformity. The vacuum chamber is made of aluminum with four connections on the sides for different measurements and allowing for pumping. The permanent magnets are positioned above and below the chamber using a holder made of High Density Polyethylene (HDPE) plastic with threaded rods on the corners for height variation. The electron source chosen was a $^{113}$Sn sample with an activity of 1.0 ± 0.1 μCi. A silicon detector with three sensitive elements of 3 x 0.5 cm$^2$ each on a wafer of 1-mm thickness was used as a diagnostic detector after the device. The whole assembly was kept under vacuum of around 80 mTorr.

Energy spectra were taken with a source in line without magnets, and at an angle with magnets for comparison. The results show a selection of electrons in the lower

range of the spectrum rejecting the higher energy electrons. Preliminary performance of the prototype device is presented.

# CHAPTER 1. INTRODUCTION

## 1.1. Scientific Motivation

The detection of ionizing radiation is important in many fields. These activities include industry, education, fundamental research, safety, and security. Devices that detect radiation must be built to ensure trustworthy measurements of the surrounding radiation. Thus, it is important to characterize the detector response to different types of ionizing radiation. General properties of interest for a detector or detector system are the energy resolution and detection efficiency. Energy resolution describes how well the detector can measure the energy of incident radiation. Detection efficiency provides information on the probability of obtaining output for each quantum of radiation that interacts with the detector volume. Such properties can be studied for each type of radiation (alpha, beta, gamma, and neutron).

In this case, the project is concerned with electrons between 100 keV and 1 MeV. Electrons with these energies can be used to characterize detectors used in beta decay experiments, such as scintillation detectors. The use of radioactive sources is convenient to make the device table-top. The radius of curvature chosen is 2 inches. The magnetic field required to separate the lower end of this energy range corresponds to a couple of hundred gauss. Desirable intensity is in the range of 1 to 100 Hz.

Among the ways of producing electrons in the laboratory one is through radioisotope sources. There are three common mechanisms of electron production from radiation sources: Beta decay, Internal Conversion, and Auger Electrons. Beta decay

produces electrons over a continuous range energy, while the other two processes are discrete and yield electrons with specific energies. Therefore, using radioisotope sources for the characterization of detectors entail limitations as to the selection of a specific energy on which to assess the detector properties.

Apart from radioisotope sources, modern accelerators are also available to produce electrons with a range of energies. An accelerator produces ions by means of a cathode or a plasma to be accelerated downstream by a potential difference of appropriate polarity [1]. To prevent divergence, magnetic and electrostatic lenses are employed along the beam line. This is how electrostatics accelerators such as the x-ray tubes, Cockcroft-Walton electrostatic accelerators, and Van de Graaff accelerators were developed [2].

According to Lee, accelerators were developed to study the structure of matter and the nucleosynthesis of elements in the early Universe [2]. Even the low-energy accelerators produce beams in the 10-100 MeV range [3]. Applications are also found in industry. This option offers the advantage of producing electron beams of specific energy. However, in many cases, these energies are rather too high, on the order of GeV, for the purpose of detector studies. In the case of small electron accelerators, often commercially available, such as x-ray machines, the electrons need to be accelerated, while with a radioisotope they are already ejected with large momenta (keV-MeV). Additionally, these accelerators facilities cannot produce low intensity electron beams (~ 1 – 100 Hz) suitable for detector characterization.

Thus, it would be desirable to develop a monoenergetic electron separator using a radioisotope source of small laboratory scale with the capability to vary the energies of the beam. In this chapter, we discuss the electron emission via radioisotope decay (Section 1.2), electron detector properties (Section 1.3), principle of device operation (Section 1.4), and the scope of the project (Section 1.5).

## 1.2. Electron Emission from Radioisotope Decay

The production of electrons from long-lived radioisotopes occurs through several different mechanisms. The most commonplace source is a radioactive element that decays through beta-minus ($\beta^-$) emission according to

$$ {}^{A}_{Z}X \rightarrow {}^{A}_{Z+1}Y + \beta^- + \bar{\nu}_e \quad (1) $$

Where $X$ is the parent nucleus, $Y$ the daughter nucleus, and $\bar{\nu}_e$ is an antineutrino, *A* the mass number, and *Z* the atomic number of the parent.

Among the products of this reaction, the only one of consequence is the electron. The antineutrino is almost massless and hardly interacts with matter, and the daughter nucleus receives a very little recoil energy that rarely leaves the source material. It is also noteworthy that after this reaction takes place, the daughter nucleus may be in an excited state, that can de-excite by emitting gamma rays. These photons can potentially pose a problem and could provide an unwanted background to the detector being characterized. If this were the case, there would have to be a shield made of lead to deal with these gammas.

As for the spectrum of energies, since the decay energy is mainly distributed between the electron and the antineutrino, the resulting distribution is a continuous curve that goes from zero to a maximum value known as the beta decay *Q* value ($Q_{\beta^-}$). The *Q*-value is equal to the difference between the initial and final nuclear mass energies [3]. A typical spectrum is shown in Figure 2. Common long-lived nuclides that decay thorough this mechanism include $^{36}Cl$, $^{137}Cs$, and $^{90}Sr$.

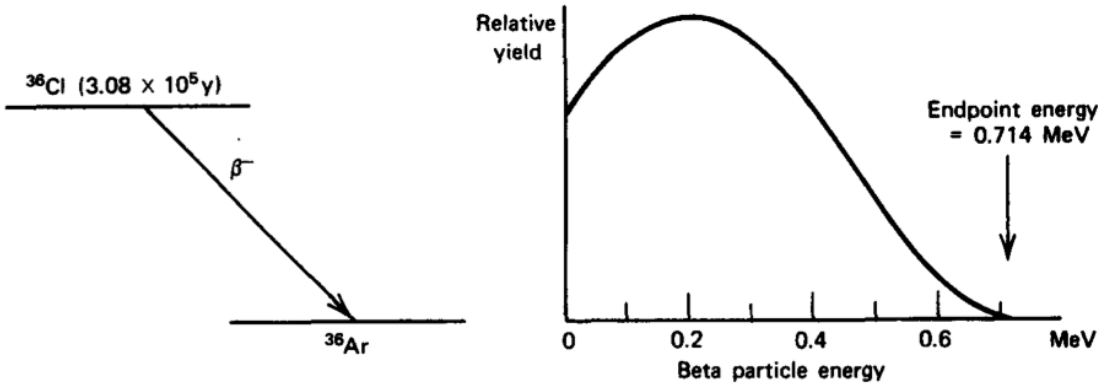


Fig. 1. Beta decay scheme and energy distribution of $^{36}Cl$. Figure from Ref [4].

Given such a variety of energies coming from one source, it is evident that this type of nuclide is immediately ruled out as a source of monoenergetic electrons.

Monoenergetic electrons can be produced by a different process called internal `conversion. This process is of an electromagnetic nature. In this case, the excited nucleus, instead of emitting gamma rays, transfers its energy to an atomic electron that is ejected with an energy given by the difference between the initial and final nuclear states and the binding energy of the orbital electron. This is more common in the heavy nuclei where the electromagnetic fields of the nucleus are strong enough to affect the inner orbit of atomic electrons [5]. An example of spectrum is shown in

Figure 3. Examples of nuclides that yield conversion electrons in their decay are $^{113}$Sn and $^{207}$Bi.

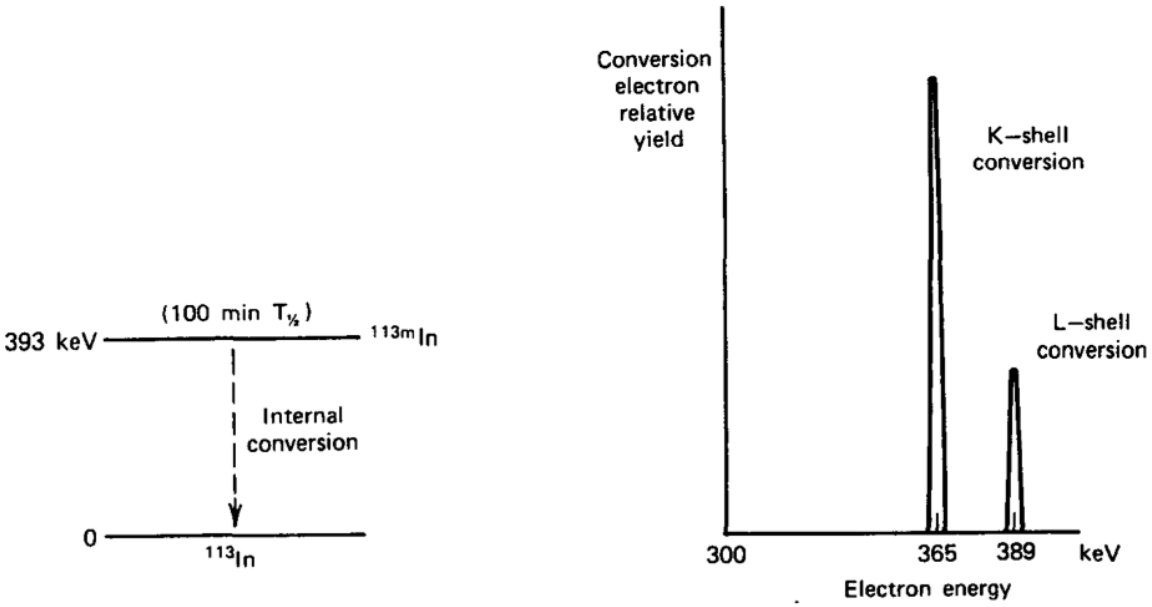


Fig. 2. Diagram of conversion electron energies from the decay of the 393-keV isomeric state in $^{113m}$In. Figure from Ref [4].

A shortcoming of this process is that even though a nearly monoenergetic electron is produced in each conversion, the same excited state could eject other electrons from nearby orbitals with different energies. In addition to this, there could be more than one excited state to go into conversion. The energy and the probability of emission are dictated by both the nuclear and atomic structure of the daughter nucleus, making it impossible to tune them.

The third mechanism is Auger electron emission. Contrary to conversion electrons, where the excitation is in the nucleus, this process originates from atomic excited states. Instead of returning to the ground state by emitting a photon, the energy is transferred to an electron that is ejected with a specific energy. Typical energies

range from eV to some tens of keV. This range falls below the region of interest between 100 keV and 1 MeV.

### 1.3. Electron Detector Properties

Common properties of detectors to characterize are the energy resolution and detector efficiency. The energy resolution measures how well a detector can distinguish between different energies. This is better illustrated in Figure 1.

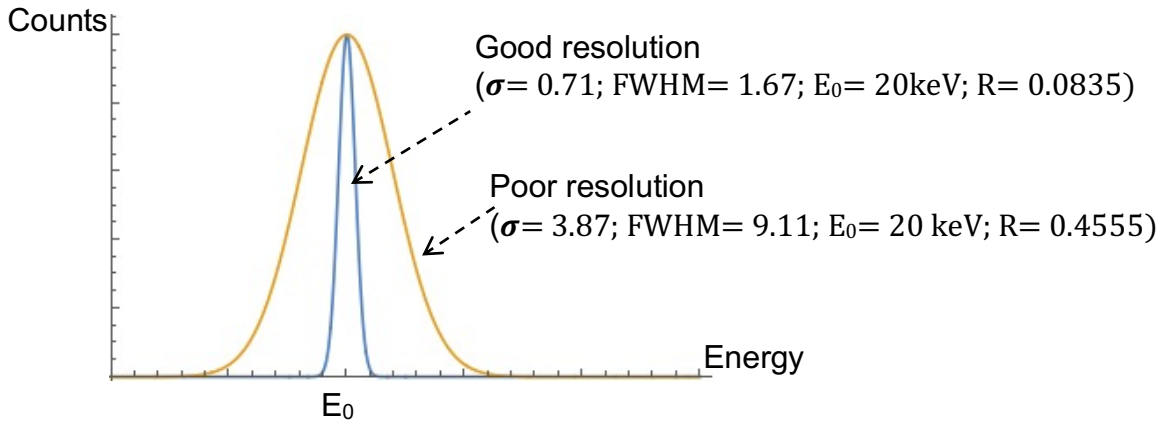


Fig. 3. Plot comparing detector energy resolution. For the same energy peak $E_0$, the good resolution presents less spread, whereas the poor resolution is wider encompassing more values of energy and therefore making it harder to distinguish between close values of energies. $\boldsymbol{\sigma}$ is the standard deviation and FWHM is the full with at half maximum.

Mathematically, the energy resolution is defined as the full width at half maximum (FWHM) divided by the position of the peak centroid $E_0$ [4].

$$R = \frac{FWHM}{E_0} \tag{2}$$

The smaller this figure, the better the detector will be at resolving different energy

electrons. For example, the resolution of semiconductor detectors for alpha spectroscopy can be less than 1%, and that of organic scintillation detectors for electron spectroscopy is in the range of 5-10% [4].

In terms of detector efficiency, this property measures the amount of output for each particle that interacts with the sensitive volume of the detector. In the case of charged particles such as alphas and electrons this interaction is through ionization or excitation giving a good response like in the case of ionization chambers and scintillation detectors. On the other hand, uncharged particles such as gamma rays and neutrons have a longer path in the volume before being detected and therefore have lower efficiency.

Formally, the efficiency (absolute) is defined as the number of events recorded divided by the number of energy quanta emitted by the source,

$$\epsilon_{abs} = \frac{number\ of\ events\ observed}{number\ of\ radiation\ \ quanta\ emitted\ by\ the\ source} \tag{3}$$

The intrinsic efficiency is defined by number of events recorded over the number of energy quanta that make it to the detector,

$$\epsilon_{int} = \frac{number\ of\ events\ observed}{number\ of\ radiation\ \ quanta\ on\ the\ detector} \tag{4}$$

This number will change with electron energy. Higher energy electrons can scatter out of the detector, whereas low energy electrons might produce a signal, but be the same as the noise.

These properties are ideally tested with a monoenergetic electron source. The energy resolution is tested by recording a spectrum to find the peak and the FWHM, and then dividing it by the position of the peak. The detection efficiency is tested on the other hand by counting the number of events on the detector divided by the number of radiation quanta emitted by the source. However, the available sources like the beta-decay nuclides are not monoenergetic; the conversion electron radioisotopes are not variable in energy, and most accelerator are not readily accessible.

Therefore, the development of a table-top device with tunable energy offers a solution to these problems. An apparatus like this could be used constantly in the laboratories for testing purposes without having to rely on external factors to schedule work. Furthermore, this device could also be useful not only in nuclear and particle physics, but also in applied fields such as medical physics.

### 1.4. Principle of Device Operation: Electron Optics

Electron beams traveling in space can be described similarly to electromagnetic radiation in terms of deflection effects due to lenses. In the case of light, physical lenses are used to bend rays and focus them into an image. This is also the case for electron beams where instead of optical lenses, electric or magnetic lenses are used. For this reason, many of the concepts studied in light optics are applied in ion optics.

The movement of charged particles in magnetic fields is governed by the shape of the fields and the characteristics of the particle, such as its mass, charge, and

velocity. The fields are described by Maxwell laws and the motion of the particles is described by the Lorentz force. In the case of electrons, they are sensitive to small electric and magnetic fields due to their small mass and charge ($m_e/e$).

In radioactive decay, electrons leave the source with an energy that makes its speed comparable to the speed of light. The total energy is the rest energy plus the kinetic energy,

$$E = m_0 c^2 + K \tag{5}$$

where $m_0$ is the mass of the electron at rest; $c$, the speed of light, and $K$, the kinetic energy. In this case, relativistic considerations have to be taken into account. This affects the mass of the electrons according to

$$m = \gamma m_0 = \frac{m_0}{\sqrt{1-(v^2/c^2)}} \tag{6}$$

where $m$ is the relativistic mass of the electron, and $v$, the speed of the electron. As the electron moves forward and enters the region of the magnetic field, its trajectory is changed due the Lorentz force.

$$\vec{F} = e\vec{v}\times\vec{B} \tag{7}$$

This force is perpendicular to the direction of the field and the velocity,

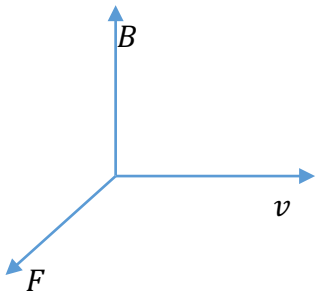


Fig. 4. Coordinate system showing the direction of $\vec{B}$, $\vec{v}$, and $\vec{F}$ for a charged particle governed by a magnetic field according to Equation 7.

Under this force, the particle accelerates and describes a trajectory with a momentary radius of curvature. At this point, the Lorentz force can be equated to the centripetal force,

$$\gamma m_0 \frac{v^2}{r} = evB \tag{8}$$

where $r$ is the radius of curvature.

From this equation, the magnetic field can be determined for a given radius and energy. The magnetic rigidity is defined rearranging Equation 8,

$$\chi_B = Br = \frac{\gamma m_0 v}{e} \tag{9}$$

Particles with different rigidities will be deflected in different angles. In a constant homogeneous magnetic field all particles will move in a circular trajectory. The reference trajectory is called the optic axis, which is the line that enters and exits the magnetic sector field perpendicularly. Since not all the electrons will follow this line, some will follow a paraxial trajectory,

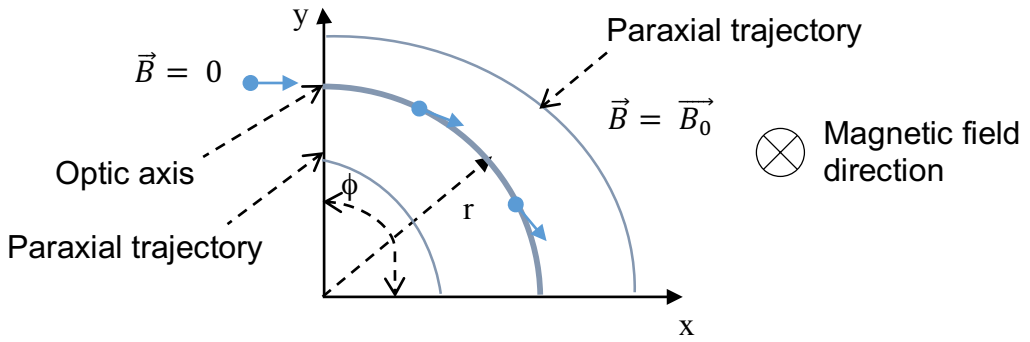


Fig. 5. Diagram showing different trajectories of electrons as they enter the region of the magnetic field. The trajectory in the middle is called optical axis, and corresponds to those electrons that enter and exit the magnet sector at a 0º angle from the faces of the magnet and are bent 90º. The other trajectories correspond to electrons entering the magnet sector with different energies.

The relation between object to image distances is, according to [6],

$$\frac{l_2}{r} = \frac{\cos\phi - M_x}{\sin\phi} \tag{10}$$

$$\frac{l_1}{r} = \frac{\cos\phi - (1/M_x)}{\sin\phi} \tag{11}$$

Where $l_1$ is the object distance; $l_2$, the image distance; $\phi$, the deflection angle; and $M_x$, the lateral magnification in the x direction which is the plane of symmetry in the middle of the sector field.

In the above figure the magnetic flux density changes abruptly from zero to a constant value. This behavior is unphysical. In reality, the sector field extends further out from the magnet plane as shown in Figure 7. The fields in this region are called fringe fields. Nevertheless, such a sudden change in the field can still be used to correctly describe first-order effects as long as an effective field boundary is determined [6].

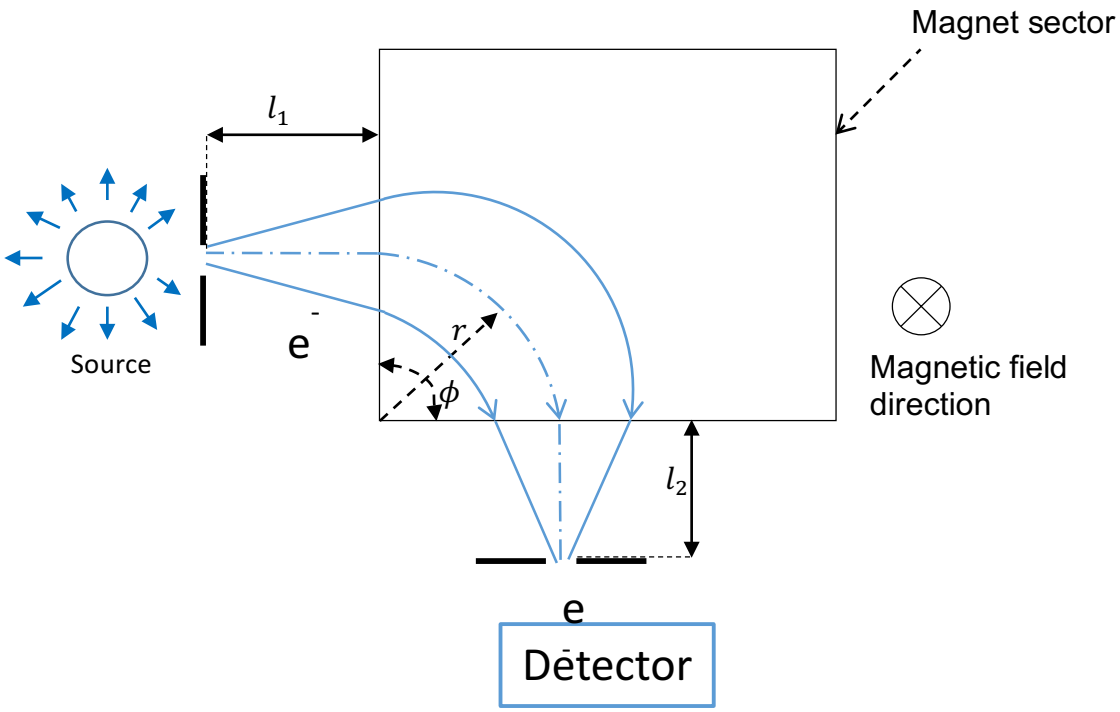


Fig. 6. Diagram showing the magnet sector field with optic axis and paraxial trajectories of electrons along with the object $l_1$, and image $l_2$ distances from the magnet.

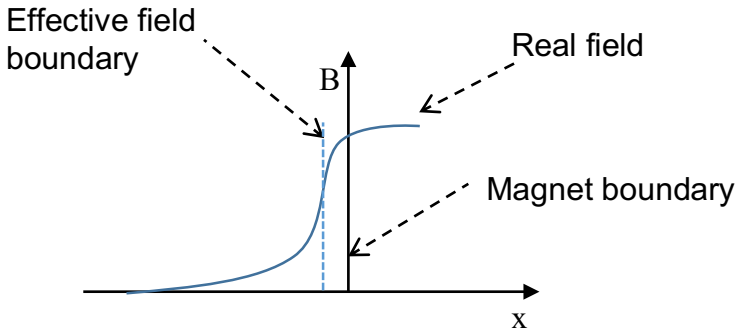


Fig. 7. Sketch showing the variation of the real magnetic field outside of magnet sector in blue solid line and the effective field boundary in blue dashed line.

By estimating the energy of the electrons coming from the source, the necessary field to deflect them can be calculated. From magnetic field measurements, the position of the effective field boundary can be determined. Then the position of the object and of the image can be obtained from Equations 10 and 11.

## 1.5. Scope of Project

The main application of the prototype device developed in this project is for the characterization of detectors. That includes the measurement of the energy resolution and the detection efficiency of scintillator and semiconductor detectors. While there are monoenergetic electron sources such as conversion electrons, they are not tunable and can feature other radiation. With this device, however, there is the option of separating electrons of specific energies, and therefore can allow for study the detector response at low energies as well.

An example of such a device is the one developed by B. Jean-Marie [7]. It consisted of a radioactive source, a vacuum chamber, permanent magnets, coils for varying the magnetic field, and magnetic shunts. The magnetic shunt is a piece of iron made to reduce the fringe fields. This device was designed for electrons in the range of 0.5 to 3.5 MeV for the study of scintillation counters and thin-plate spark chambers. It had a resolution width of 3%. The source was a 600 μCi $^{90}$Sr that gave 500 counts/s at 2 MeV [7].

In this project, since this separator is a prototype, the initial focus is to separate those electrons that follow the trajectory on the optical axis alone, and to transmit electrons through the vacuum chamber, so that further development can be confidently undertaken to accomplish a monoenergetic beam. Nevertheless, focusing effects are taken into account in order to position the source and detector in the focusing points to achieve maximum number of counts. This would allow fewer hours of operation thus increasing the efficiency.

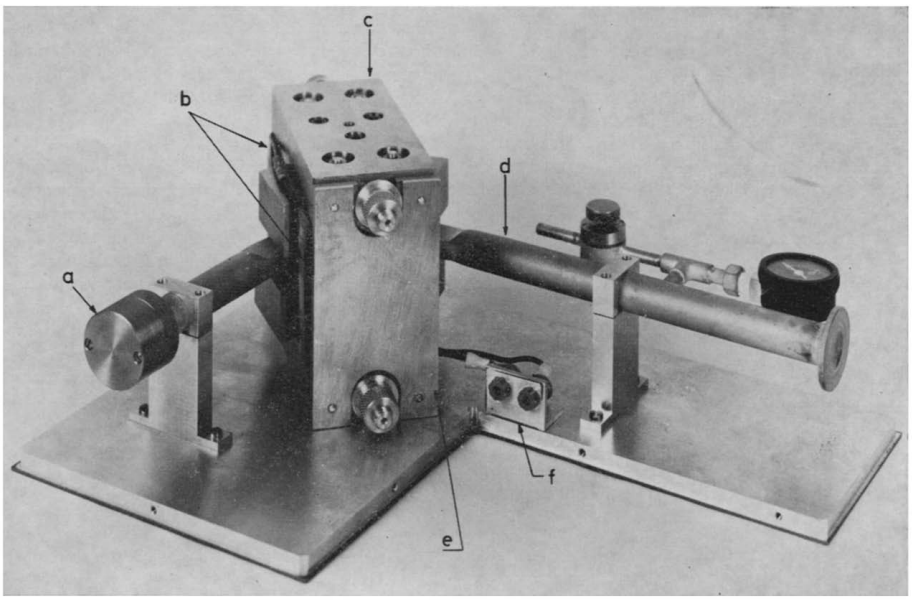


Fig. 8. Photo of the electron separator made by B. Jean-Marie. It shows a. Source, b. coils, c. permanent magnets, d. vacuum chamber, e. magnetic shunt, f. connectors. Image taken from Ref [7].

# CHAPTER 2. DESIGN

## 2.1. Source

Among the electron sources to select from there are some radionuclides that decay through beta emission and others that decay through conversion electrons. In the first case, there is a continuous spectrum with different energies and intensities. Using this type of source would allow for the selection of one particular region of the spectrum. For example, the $^{137}$Cs, with half life ($t_{1/2}$) 30.08 years, average energy ($E_{avg}$) 174.32 keV, and end-point energy ($E_{end\ point}$) of 513.97 keV gives a wide a spectrum of energies to choose from, especially in the lower range, for which is the device is intended.

On the other hand, the conversion electrons (CE) are emitted with specific energies. This makes a discrete spectrum from where to choose for the selected energies. One of the sources that emits electrons in the range of interest is $^{113}$Sn with half life 115.09 days. Specifically, conversion electrons of the K, L, and M levels, with energies 363.8 keV, 387.5 keV, and 390.9 keV, respectively [8]. For this project, the available sources from the lab are $^{113}$Sn with 1 μCi, $^{207}$Bi with 0.65 μCi, $^{137}$Cs with 20 μCi, and $^{90}$Sr with 0.1 μCi.

Although these energies are well known from theory and precise measurements, they are not the exact values that electrons have when they travel through the system. When they are produced, they have to go through the surrounding casing, thereby losing some energy. The end result is a degraded spectrum where energies are shifted towards the low-energy region and the peak is broadened. To account for this effect, calculations for the energy loss in materials have to be performed.

To estimate the energy loss, the thickness of the plastic casing is considered to be 0.5 mm. A common plastic like polyethylene has a stopping power for electrons of 2.343 MeV $cm^2/g$. With a density of 0.94 $g/cm^3$, this gives an energy loss of about 110 keV. Here already the energy of the K CE from $^{113}Sn$ decay is reduced to 254 keV. This effect adds to the different scattering throughout the material of the source and the casing, making the electrons lose less or more energy than the one mentioned above. As a result, the real spectrum measured is shifted towards lower energies with wider peaks. This effect is seen in a preliminary measurement in Chapter 3.

## 2.2. Vacuum Chamber

Since the air has its own stopping power of 2.241 MeV $cm^2/g$ for electrons of 250 keV, due to the interaction of the electrons with the gas particles, it is necessary to pump down the system and make it vacuum tight. This energy loss in air increases for low energy electrons as shown in Figure 9.

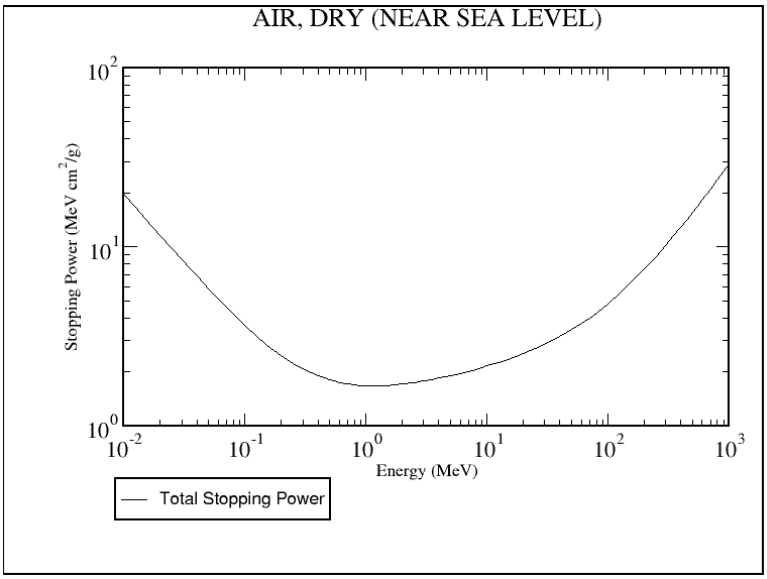


Fig. 9. Total stopping power for electrons in air. [9]

Another reason to have vacuum is to avoid a change in direction of the electrons, especially after they have been deflected by the magnet. Typical values reached with this configuration were around 80 mTorr.

The chamber is designed for a 90-degree bend and a radius of 2 inches (Fig. 10). Therefore, it has a cubic shape with holes on each side on which KF-16 pipes, centering rings, and bulkhead clamps are attached as shown in Figure 11. This would allow for comparison measurements between the source straight in front of the detector and at a 90-degree position. The material chosen is aluminum due to its low magnetic permeability and ease of fabrication.

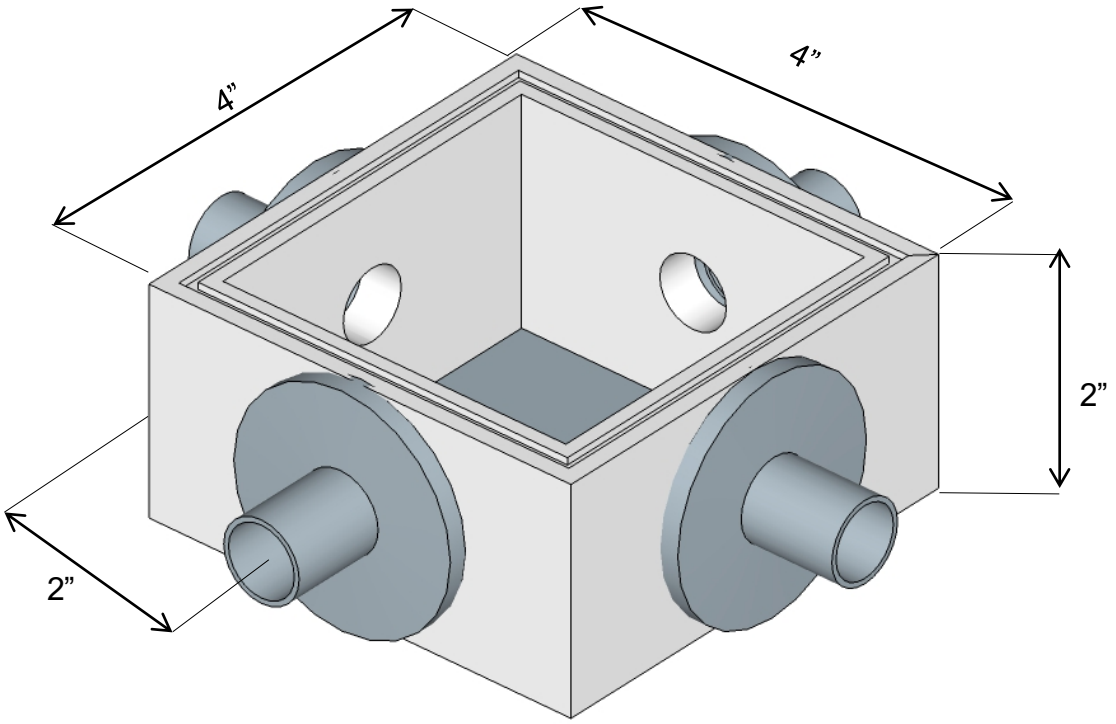


Fig. 10. Design of the interior of the separator vacuum chamber. The material chosen is aluminum due the its low permeability. The four holes on the sides allow for different positions of the source, alignment, as well as pumping. The dark grey pipes show approximately the dimensions of KF-16 pipes clamped down to the exterior.

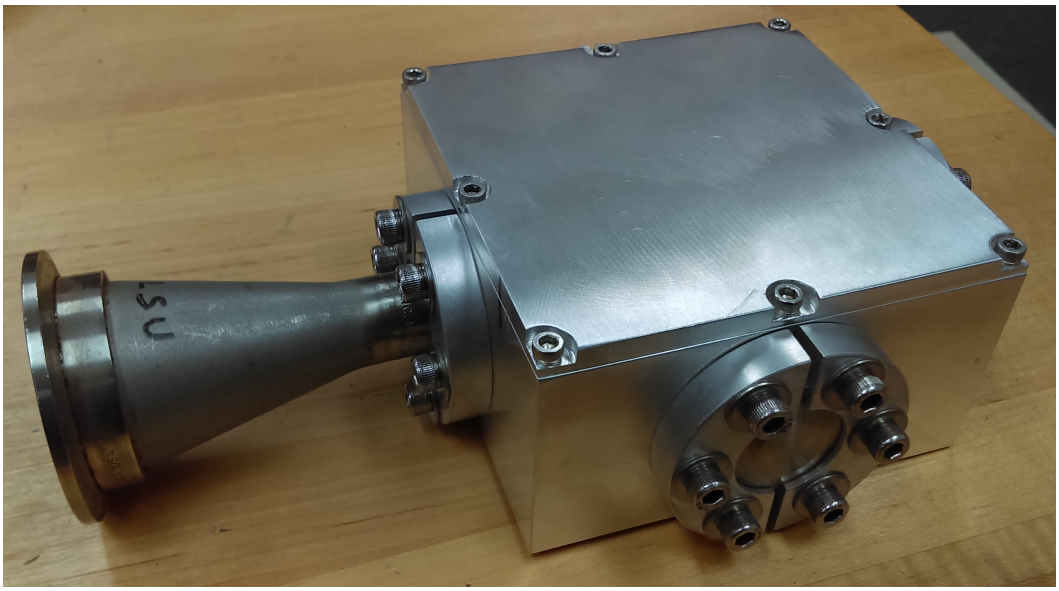

Fig. 11. Picture of the vacuum chamber built for the project, made of aluminum, and showing the KF-16 pipe, centering ring, blank, and bulkhead clamps. The blanks can be removed to connect the pump and the end line of the system. The top flange this bolted down to the base with 4-40 bolts and a custom o-ring in between.

### 2.3. Permanent Magnets

The permanent magnets are the heart of the prototype device, for they are responsible for creating field that deflects the electrons. Therefore, in order to have the appropriate magnetic field strength we need to take into account the energy of the electrons. In this case, we considered energies in the range of 100 keV to 1 MeV. This would allow us to use the device for different sources like $^{113}$Sn, $^{207}$Bi, and $^{90}$Sr, which produce electrons in the region.

According to the calculations, the field values corresponding to those energies go from 220 to 933 gauss. Available permanent magnets in the market deliver this range of strength for residual induction ($B_r$) of 3900 gauss, with dimensions of 6” by 4”, thickness of 0.250”, and varying separation from 3.04” to 2.30” (height of chamber including top flange), calculated using Equation 12. For stronger field the magnets can be stacked up. This separation is attainable through a special holder

with four threaded rods on each corner along with hex nuts (Figure 12 and Figure 13). The expression of the magnetic field between two rectangular magnets is expressed by

$$B_z = 2\frac{B_r}{\pi}\left[\tan^{-1}\left[\frac{AB}{2X\sqrt{4X^2+A^2+B^2}}\right] - \tan^{-1}\left[\frac{AB}{2(L+X)\sqrt{4(L+X)^2+A^2+B^2}}\right]\right] \quad (12)$$

where *A* is the length, *B* the width, *L* the thickness, and *X* the distance from the magnet.

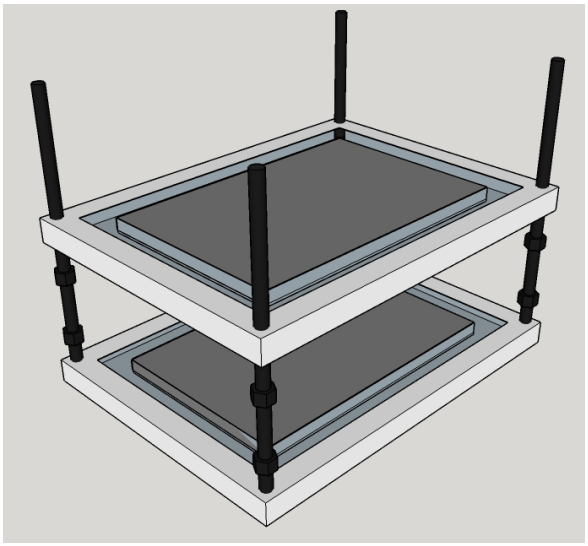

Fig. 12. Design of the magnet holder. The lower and upper holders are made of HDPE plastic (white). They are held together through threaded plastic rods and nuts in each corner (black). The magnets (grey) are placed in beds milled out in the upper and lower plastics.

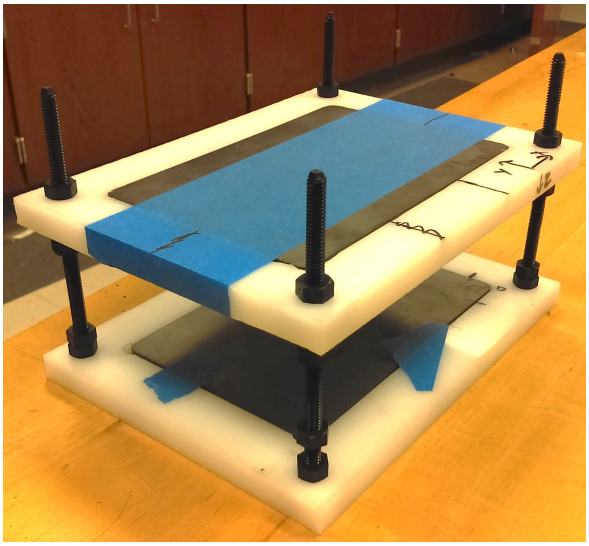

Fig. 13. Picture of the actual magnet holder. The upper and lower holders are made of HDPE (White). The pockets were milled out using a mill and cutter bits to the exact dimensions of the magnets (Grey). The threaded rods are placed on the four corners and allow for height variation through hexagonal nuts.

Apart from the theoretical calculations, it was necessary to perform an experimental measurement of the field between the magnets. For this purpose, measurements with an F.W. Bell model 5180 gaussmeter with a ST018-0404 Transverse Hall Probe of all three planes at different heights and for different magnet separations were performed. This was made using the bed of an end milling machine. The movement mechanism through the handwheel and dial were used to map the field at steps of 0.5” throughout planes between the magnets. A subset of results is shown in the Figures 14 and 15.

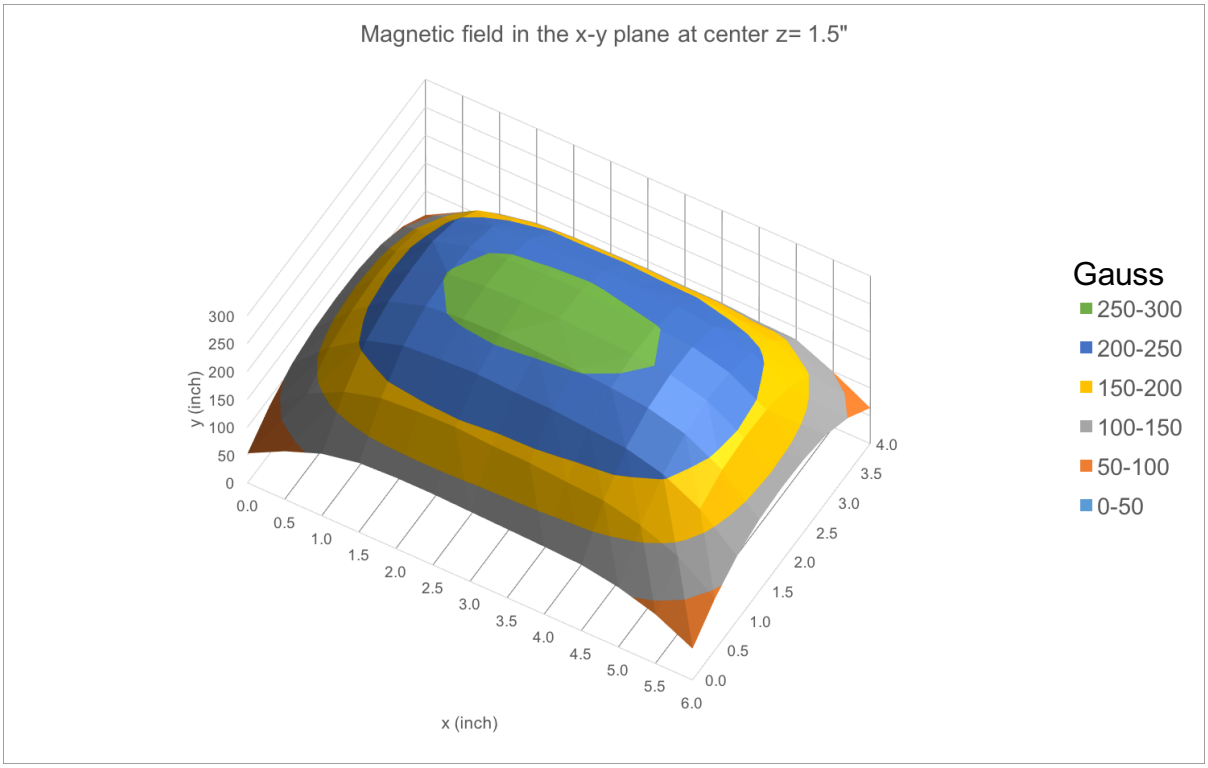


Fig. 14. Magnetic field profile of $B_z$ at 1.5” for a magnet separation of 3”.

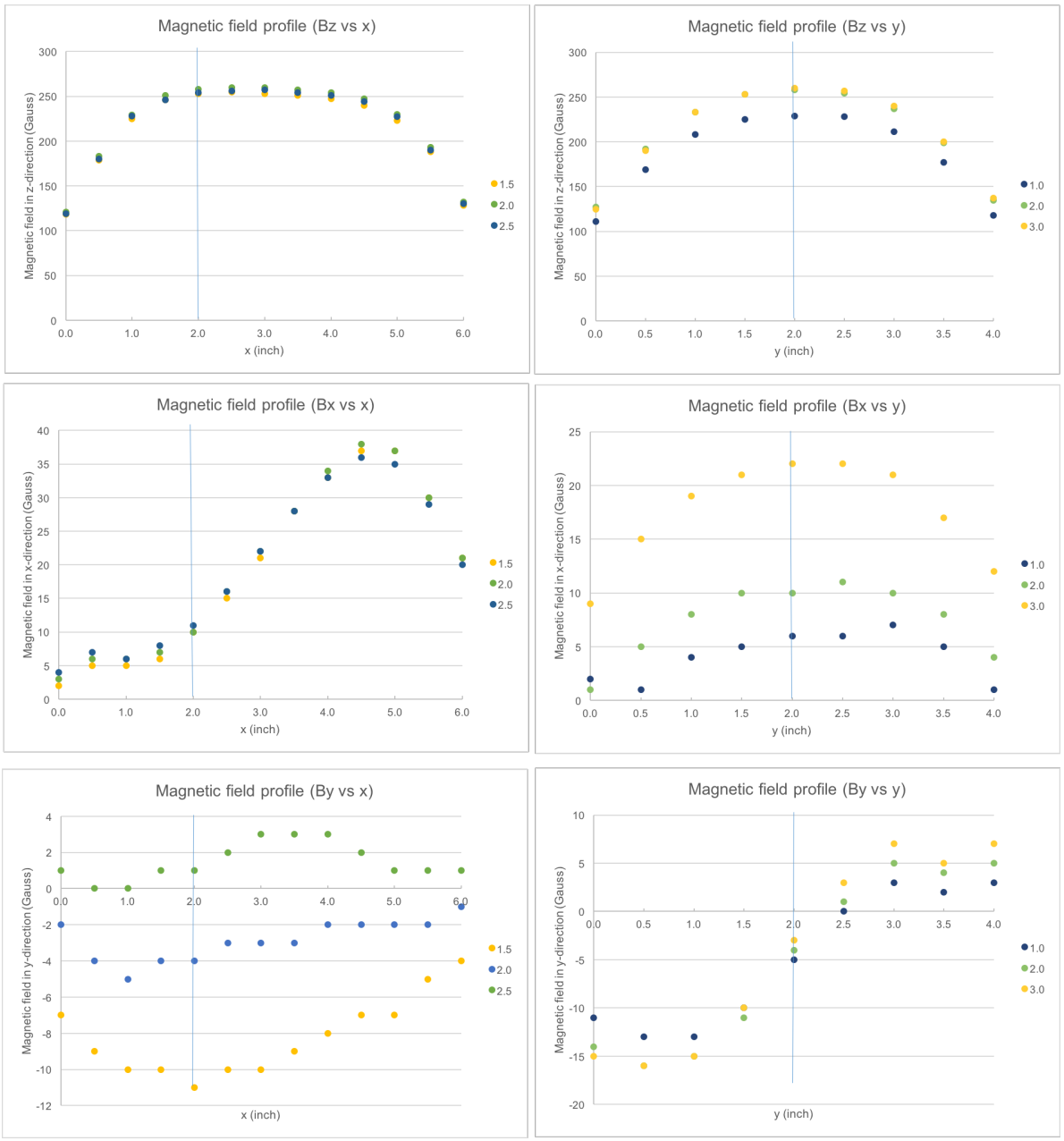


Fig. 15. Plots showing profiles of $B_z$, $B_x$ and $B_y$ along the middle length and width of the magnet array for a separation distance of 3". The profiles for y = 1.5", 2.0", and 2.5" and for x = 1.0", 2.0" and 3.0" are shown to show the variation in the corner region of the magnet. The uncertainty in the in the x-y measurement is 0.001", and the uncertainty in the field measurement are 2% for B > 33.0 gauss, 3% for 33 > B ≥ 18 gauss, 5% for 18 > B > 10 gauss, ~ 10% for B ~ 5 gauss, and ~ 40% for B ~ 1 gauss. These components have an effect on the path of electrons deviating them from a circular path. The blue line shows the position of the pipe.

From these profiles it is possible to see the uniformity of the field. As it is shown in the $B_z$ plots, there is little change around 250 gauss at the center region of the magnet. The $B_x$ and $B_y$ plots help to choose the part where the lateral fields are at a

minimum. This corresponds to the corner with coordinate x= 2, y= 2. Therefore, placing the chamber at this corner will reduce the effect of lateral fields. The object distance, $l_1$, and the image distance, $l_2$, are both 2". They were calculated using equations 10 and 11, and setting the lateral magnification $M_x$ equal to -1.

### 2.4. Diagnostic Detectors

Since the objective of the device is to create a monoenergetic source of electrons, the only way to test it is by measurement with a diagnostic detector with good energy resolution. The detector employed is a silicon detector developed for the Atlas Positron EXperiment (APEX) at Argonne National Laboratory. It consists of three 3 x 0.5 $cm^2$ elements on a wafer of 1 mm thickness. The form is trapezoidal with length 31.75 mm, top width 15.5 mm, and bottom width 19.18 mm as shown in Figure 17. 500 keV electrons are fully stopped in the material, whereas for 1000 keV, only 30% of those incident are fully stopped [10].

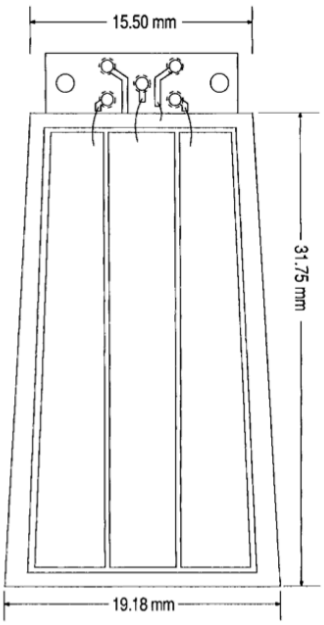


Fig. 16. APEX silicon detector layout. Figure taken from Ref [10].

According to Evensen et al., this detector has a resolution of 3 - 4 keV FWHM at 481 keV at room temperature [10]. This resolution is enough to determine how well the separator works. The aim is to use the separator to test the response of scintillator detectors which have poor resolution, but very good detection efficiency. Figure 18 shows a spectrum of $^{207}$Bi obtained with one of the detectors.

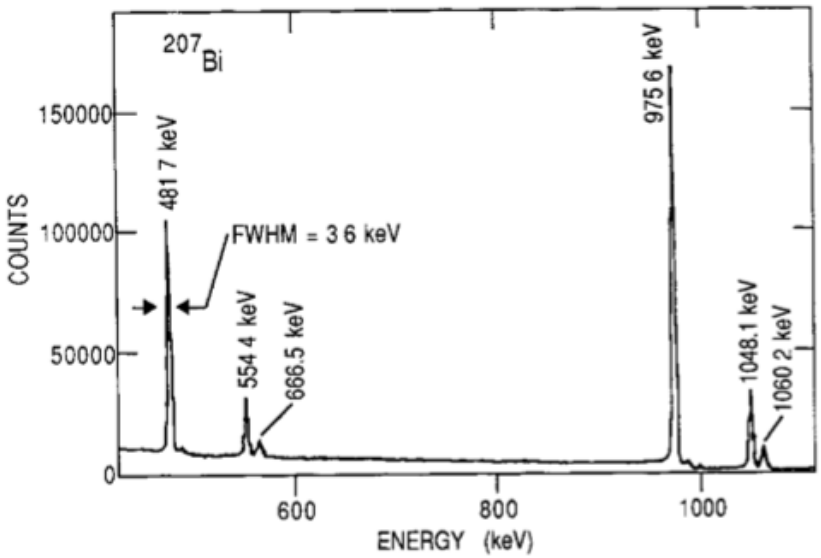


Fig. 17. Spectrum of conversion electrons from $^{207}$Bi decay showing the resolution of 3.6 keV FWHM at 481.7 keV [10].

The detector was connected using a feedthrough, a preamplifier, an amplifier, an Analog-to-Digital Converter (ADC) and a CPU as shown in Figure 19.

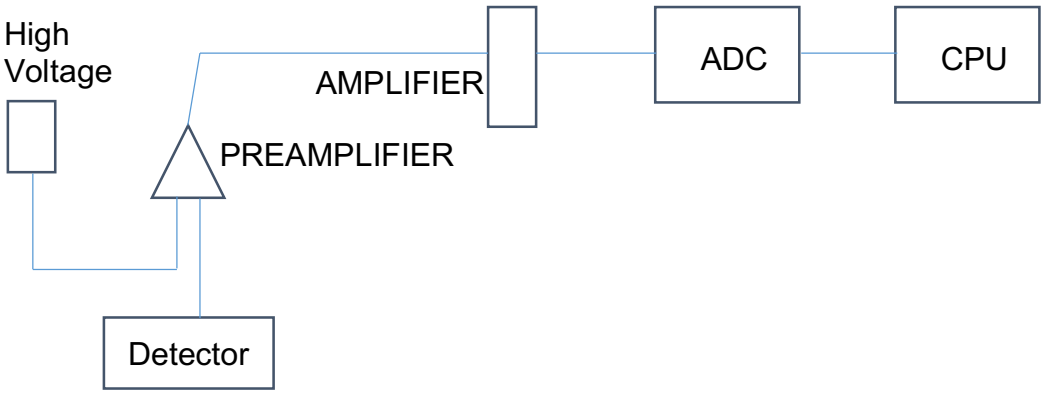


Fig. 18. Electronics diagram for the diagnostic detector.

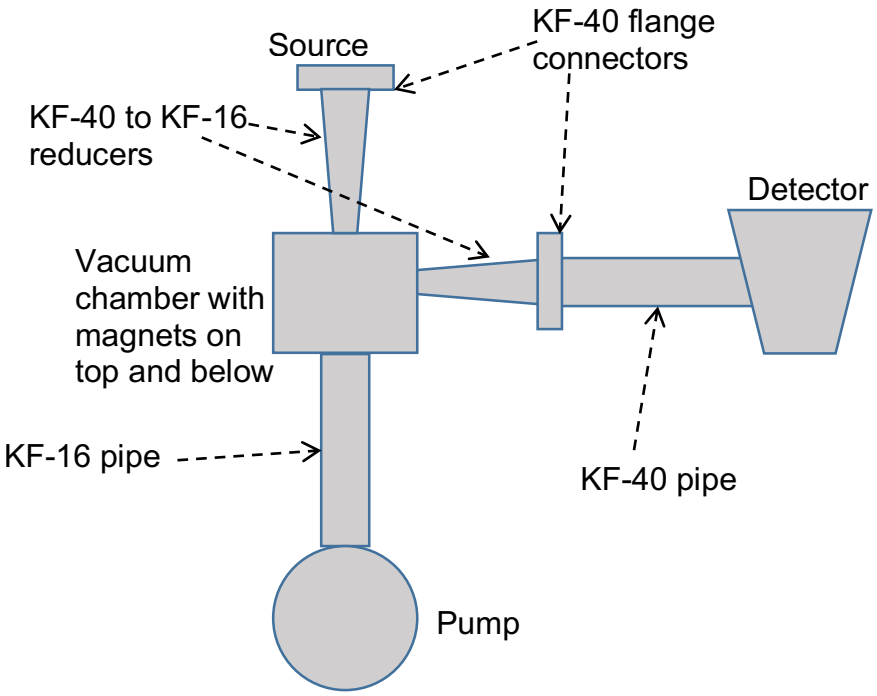


Fig. 19. Sketch of vacuum components of prototype electron separator.

CHAPTER 3. PRELIMINARY MEASUREMENTS

Different measurements were taken with the $^{113}$Sn source at 0º position relative to the detector without the magnet array and at 90º position with the magnet array, respectively. All measurements were taken with a brass collimator 0.75mm thick, and with an aperture of 1.5mm located at the calculated distance $l_1$ = 2”. For the position at 0º, in general, a broader energy spectrum was obtained. This is an expected result since there is no selector element between the source and the detector. On the other hand, when the source was placed at a 90º angle with the magnets in place, there was a reduction on the higher energy electrons. This is better seen in the following figures.

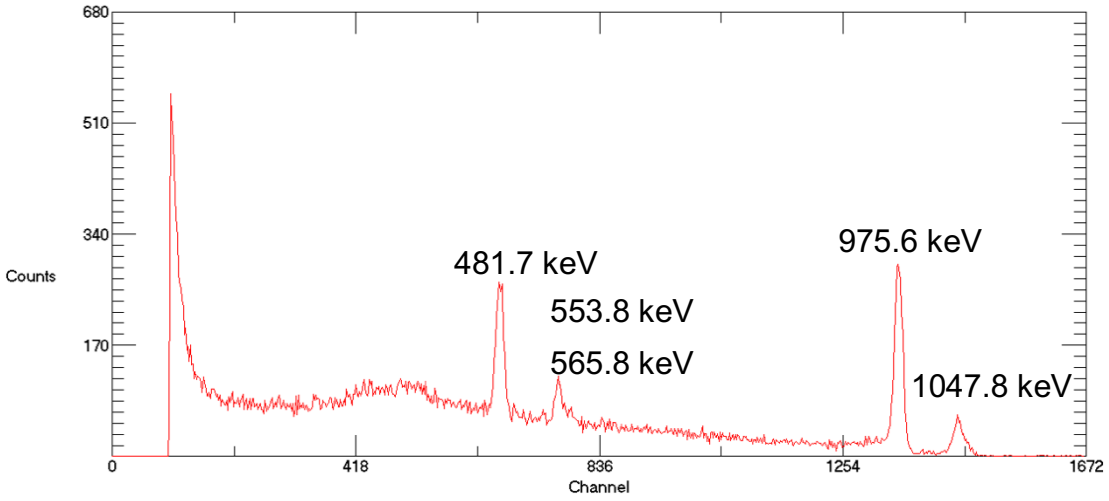


Fig. 20. Plot the spectrum of $^{207}$Bi used for calibration. Measured for 3600 s real time and at a detector bias -150 V.

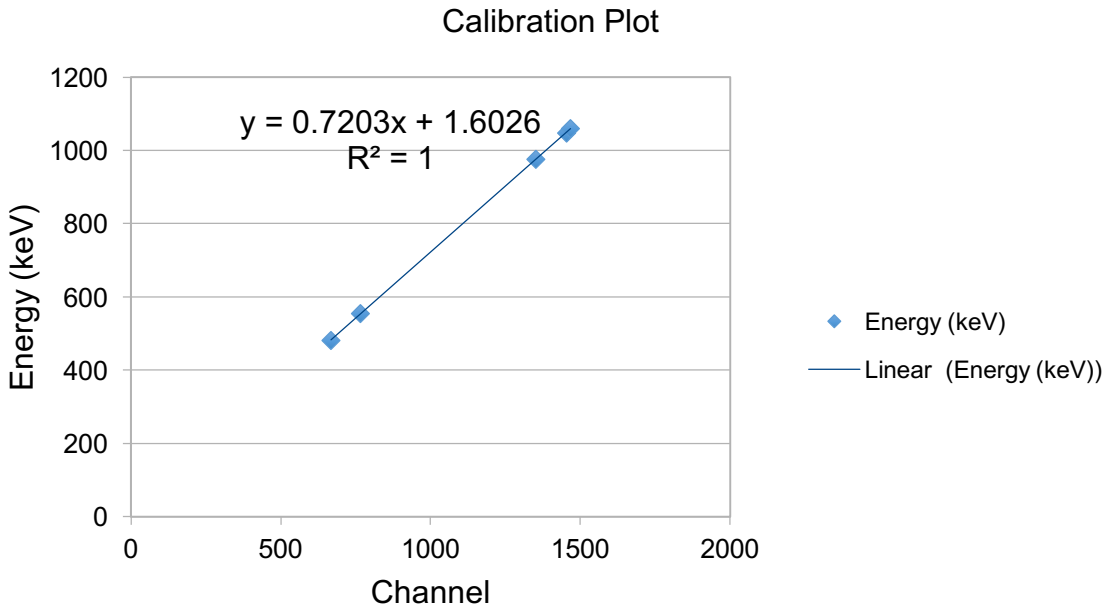


Fig. 21. Calibration plot from the $^{207}$Bi spectrum.

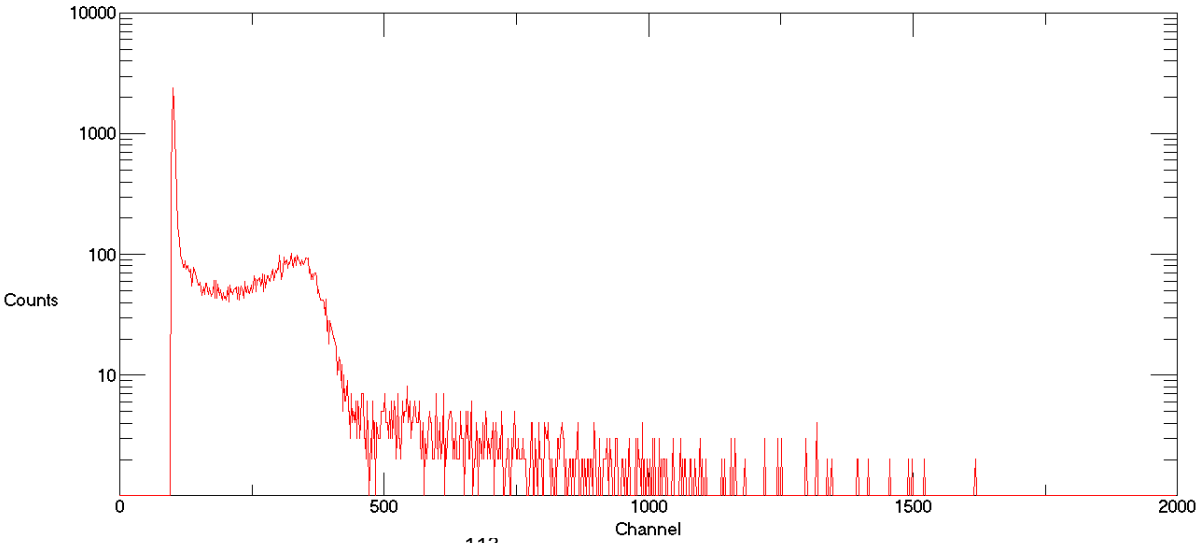


Fig. 22. Plot of the spectrum of $^{113}$Sn at 0º with no magnets in place. Measured for 45000 s real time and at a detector bias -150 V.

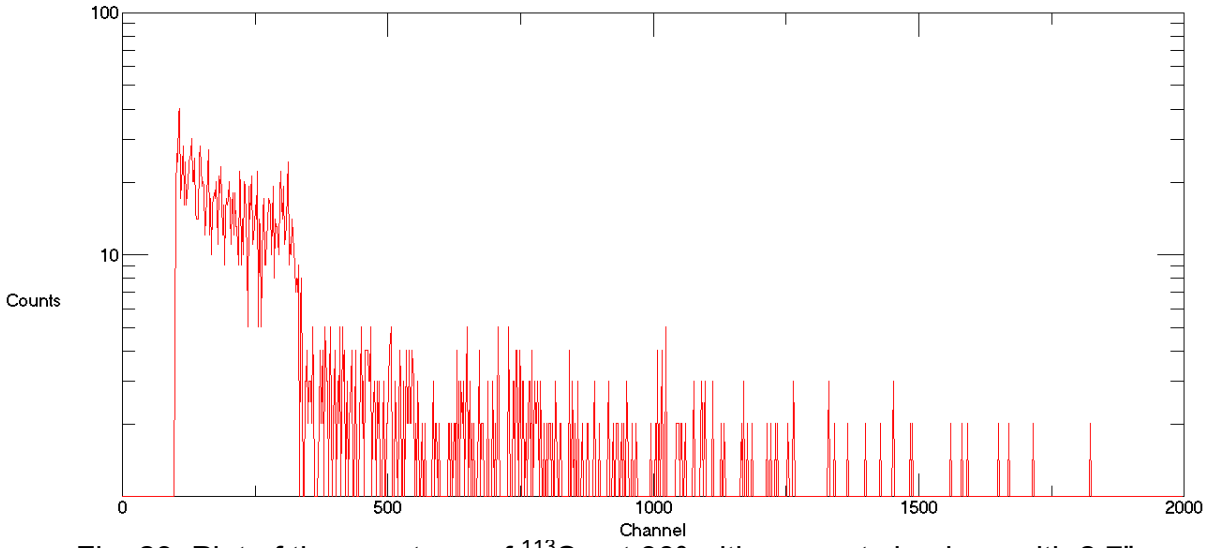


Fig. 23. Plot of the spectrum of $^{113}$Sn at 90º with magnets in place with 2.7" separation. Measured for 45000 s real time and at a detector bias -150 V.

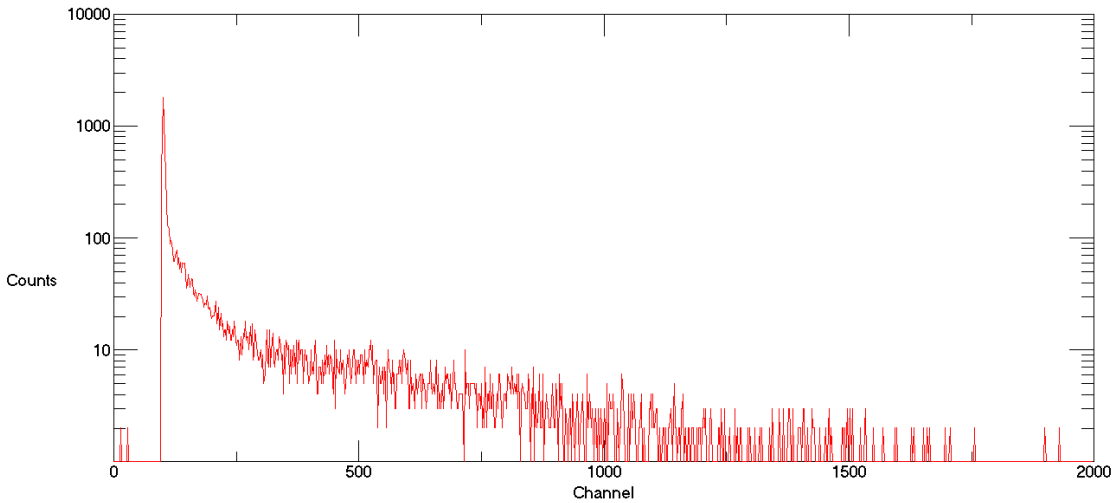


Fig. 24. Plot of the background spectrum. Measured for 87788 s real time and at a detector bias -150 V.

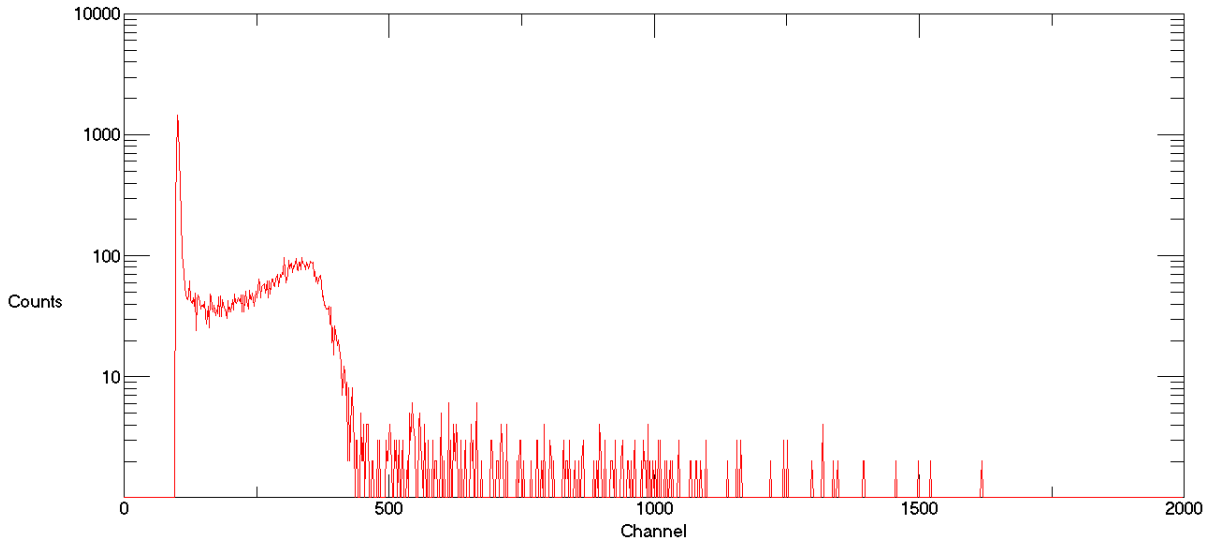


Fig. 25. Plot of the spectrum of $^{113}$Sn at 0º with no magnets in place and background subtracted. Measured for 45000 s real time and at a detector bias -150 V.

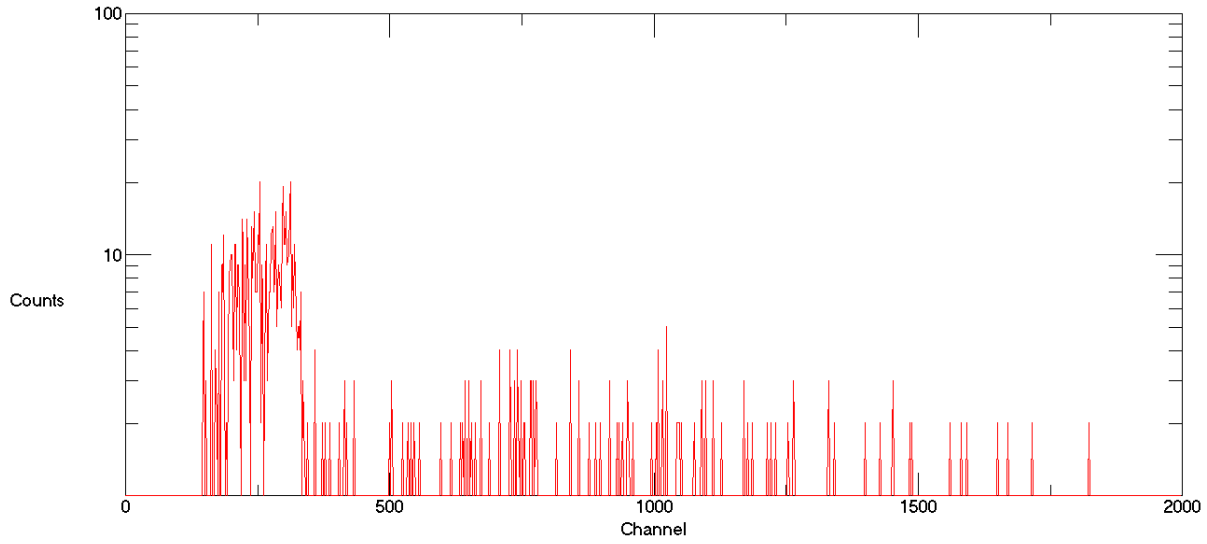


Fig. 26. Plot of the spectrum of $^{113}$Sn at 90º with magnets in place with 2.7" separation (260 < $B_z$ < 346 gauss) and background subtracted. Measured for 45000 s real time and at a detector bias -150 V.

# CHAPTER 4. CONCLUSION

The detection of radiation is very important in different fields such as research, industry and medicine. In order to properly measure this radiation, the detectors employed have to be characterized ideally for different values of energies. However, due to the limited values of energies provided by naturally available electron sources such as radionuclides it was envisioned the construction of a prototype device capable of separating electrons of a range of energies that can be further improved in future work to narrow down the range to a monoenergectic beam.

With this motivation, the first steps were the theoretical calculations in order to obtain the dimensions of the different components. This encompassed from the energy loss in casing material to the distances of the object and of the image. In order to inspect for uniformity of the magnet, a mapping of the field at different distances was performed. When all the parts were fabricated and assembled, electron energy measurements were taken at source positions 0º (without magnets) and 90º (with magnets) relative to the diagnostic detector.

Results for $^{113}$Sn show that electrons between 100 keV and 240 keV make it through the 90º bend with the magnets in place and a separation of 2.7”. This was obtained for a running time of 45000 s and the detector biased at -150 volts. No collimator at the image position $I_2$. This result is encouraging since this prototype device was intended to separate electrons and bend them through the vacuum chamber. From this stage, further work can be confidently taken in order to obtain a monoenergetic spectrum.

To accomplish this goal, plans for the future include computer simulations of the electrons path through the magnetic field ($e^-$ in $B_x$, $B_y$, $B_z$), measurements with a stronger electron source, attain higher accuracy/precision of the magnetic field measurements, improved collimation of the electron source, and the development of electromagnetic coils to replace the permanent magnet array.

# REFERENCES


[1] M. Reiser, *Theory and Design of Charged Particle Beams* (Wiley-VCH, Weinheim, 2008).

[2] S. Y. Lee, *Accelerator Physics* (World Scientific Publishing Company, New Jersey, 2004).

[3] K. S. Krane, *Introductory Nuclear Physics* (John Wiley & Sons, 1988).

[4] G. F. Knoll, *Radiation Detection and Measurement* (John Wiley & Sons, 2010).

[5] S. S. M. Wong, *Introductory Nuclear Physics* (Wiley-VCH, Weinheim, 2004).

[6] H. Wollnik, *Optics of Charged Particles* (Academic press, 1987).

[7] B. Jean-Marie, Nuclear Instruments and Methods 75, 287 (1969).

[8] Nuclear Data Sheets 111, 1471 (2010)

[9] Physical Measurement Laboratory.
http://physics.nist.gov/PhysRefData/Star/Text/ESTAR.html

[10] L. Evensen, A. Hanneborg, T. Happ, A. H. Wuosmaa, and R. Betts, Nuclear Instruments and Methods in Physics Research Section A: Accelerators, Spectrometers, Detectors and Associated Equipment 326, 136 (1993).

# VITA

Sergio López received his Bachelor of Science from Universidad Nacional de Asunción in 2007. Afterwards he made the decision to enter graduate school in the Department of Physics and Astronomy at Louisiana State University. He hopes to receive his Master's degree in 2017.